DOI: 10.26565/2312-4334-2026-3-48 ISSN 2312-4334

THEORETICAL AND EXPERIMENTAL ANALYSIS OF RAYLEIGH–TAYLOR INSTABILITY AND MARANGONI CONVECTION IN COPPER FOIL UNDER LASER IRRADIATION

M.M. Akhmedov[1*], **J.O. Sadullayev**[1], **M.E. Vapayev**[1], **N.P. Babayazova**[1], **A.R. Matnazarov**[2], **I.Y. Davletov**[1], **M. Jumaniyazova**[3], **R.O. Ozodov**[4], **B. Ismatov**[5], **F.J. Matchanova**[6]

[1]*Deparment of Technique, Urgench State University named after Abu Raykhan Beruni, Urgench, 220100, Uzbekistan*
[2]*Urgench Innovation University, st. Town Independence MFY, 2nd House, Urgench, 220100,Uzbekistan*
[3]*Department of Physics and Astronomy, Urgench State Pedagogical Institute, 1-A, Gurlan Str., Urgench city, 220100, Uzbekistan*
[4]*Department of Biophysics, Physical Culture and Sports, Urgench State Medical Institute, Al Khorezmi Street 2, Urgench city, 220100, Uzbekistan*
[5]*"Tashkent Institute of Irrigation and Agricultural Mechanization Engineers" National Research University, Kori Niyoziy 39, Tashkent, 100000, Uzbekistan*
[6]*Khiva district general secondary school No. 10 Sakhovat Street 98, Khiva district, 220900, Uzbekistan*
[*]*Corresponding Author e-mail: munisbek95@urdu.uz*

Received April 24, 2026; revised July 31, 2026; accepted August 3, 2026

This study investigates the physical phenomena occurring on the surface of copper foil under high-intensity pulsed irradiation of a Nd: YAG laser (λ = 1064 nm, τ = 28 ps), with particular focus on plasma formation, Rayleigh–Taylor (RT) instability, and the influence of Marangoni convection on crater morphology. The plasma temperature and electron density are determined using experimental methods through spectral emission lines. These parameters evaluate the pressure gradient in the plasma, temperature variations, and changes in surface tension. The RT instability is modeled based on density contrasts arising under strong pressure differentials, while Marangoni convection is described as a mechanism for surface flow formation driven by temperature gradients. The paper analyzes the interplay between these two instabilities, their role in material redistribution, and their influence on the final geometric shape of the laser-induced crater, supported by theoretical calculations and spectroscopic measurements. The results contribute to a deeper understanding of the complex thermohydrodynamic processes involved in laser ablation.

Keywords: *Rayleigh–Taylor instability; Marangoni convection; Laser ablation; Copper plasma; Surface morphology; Electron density; Spectroscopic diagnostics*

1. INTRODUCTION

Laser–matter interaction is one of modern science's most actively developing fields, particularly within high-energy physics, materials science, and nanophotonics [1–3]. In particular, the use of ultrashort pulsed lasers (in the femtosecond and picosecond ranges) has attracted significant attention due to their ability to induce localized heating, melting, and vaporization of material surfaces, leading to plasma formation as well as the generation of craters and nano/micro-scale surface structures [4–9]. Extreme temperature gradients, pressure differences, and dynamic instabilities such as Rayleigh-Taylor and Marangoni types that arise during these processes significantly alter the surface morphology. The Rayleigh–Taylor (RT) instability occurs when high-pressure plasma layers interact with the denser metallic layer beneath them [10], leading to nonuniform material displacement at the bottom of the crater. On the other hand, Marangoni convection refers to surface fluid flows caused by surface tension gradients induced by temperature differences. The intensity of these flows is characterized by the Marangoni number (Ma), defined as:

$$\mathrm{Ma} = \frac{\left|\frac{d\sigma}{dT}\right| \cdot \Delta T \cdot L}{\mu \cdot \alpha} \tag{1}$$

where $\frac{d\sigma}{dT}$ is the temperature dependence of surface tension [N/(m·K)], ΔT is the temperature difference [K], L is the characteristic length scale [m], μ is the dynamic viscosity [Pa·s], and α is the thermal diffusivity [m²/s]. A high Marangoni number indicates the presence of strong convective flows [11], which drive the motion of molten material toward the periphery in the liquid metal layer. In recent years, several theoretical and experimental studies [12, 13, 16–22] have focused on how these instabilities affect the shape, depth, and peripheral material redistribution of laser-induced craters. Moreover, the development of spectroscopic techniques has enabled determination of plasma parameters such as temperature, electron density, and pressure gradients under realistic experimental conditions, thereby enabling more accurate modeling of the instabilities involved [23–32].

Cite as: M.M. Akhmedov, J.O. Sadullayev, M.E. Vapayev, N.P. Babayazova, A.R. Matnazarov, I.Y. Davletov, M. Jumaniyazova, R.O. Ozodov,Bakhtiyor Ismatov,F.J. Matchanova, East Eur. J. Phys. 3, 526 (2026), https://doi.org/10.26565/2312-4334-2026-3-48

In this study, for the first time, the physical processes occurring on the surface of copper foil under picosecond Nd: YAG laser irradiation are comprehensively investigated in the context of both Rayleigh–Taylor instability and Marangoni convection. Although previous studies have predominantly analyzed these phenomena separately [11–13], this article presents a unified theoretical and experimental approach. Based on the spectral characteristics of the generated plasma, a combined analysis of RT instability and Marangoni convection is carried out. The interrelations among temperature gradients, surface flows, pressure differences, and crater morphology are identified and illustrated through graphical data and experimental observations.

Besides laser irradiation, similar crater formation mechanisms have also been reported under other pulsed energy deposition techniques. Bryukhovetsky et al. [14] investigated crater formation on AA6111 aluminum alloy irradiated by a high-current pulsed electron beam and demonstrated that crater geometry is governed by non-uniform solidification of the remelted layer and the heterogeneous distribution of alloying elements. Their results indicate that material composition and crystallization dynamics strongly affect the final crater morphology. Likewise, Zhong et al. [15] studied crater formation under intense pulsed ion beam irradiation and revealed that inclusions exposed on the target surface significantly modify the melt flow through differences in the surface tension coefficient between the molten inclusion and the surrounding molten matrix. Their numerical simulations showed that thermocapillary flow driven by surface-tension differences represents the dominant mechanism responsible for crater evolution. These studies demonstrate that although the energy deposition mechanisms differ between laser, electron-beam, and ion-beam irradiation, crater formation is fundamentally governed by coupled thermal, hydrodynamic, and solidification processes.

2. EXPERIMENTAL METHODS

The experiments were carried out using commercially available high-purity copper foil (99.99 wt.% Cu) with a thickness of 63.1 μm. The high purity of the material was selected to minimize the influence of impurities on plasma formation, molten-layer dynamics, and surface-tension gradients during laser irradiation. A picosecond Nd:YAG laser (λ = 1064 nm, τ = 28 ps) operating at a laser fluence of 16 J/cm^2 was employed to irradiate the copper surface. The laser beam was focused onto the sample using a lens with a focal length of f = 25 cm. The primary objective of the experiment was to determine the plasma parameters generated during laser–matter interaction through spectroscopic diagnostics and to investigate the associated Rayleigh–Taylor instability and Marangoni convection by combining experimental observations with theoretical analysis.

Spectral analyses were performed using an Ocean Optics HR-4000 optical spectrometer. The plasma's electron density was estimated from Stark broadening of optical emission lines, while the electron temperature was determined using the Boltzmann distribution method. The crater morphology was investigated using a CX-200 scanning electron microscope (SEM), capable of magnifying up to 300,000×, allowing for high-resolution analysis of crater geometry.

During the experiment, the distribution of laser energy, spot radius, pulse repetition rate, and the optical and thermophysical properties of the material were taken into account. Figure 1 presents the experimental setup, in which the diameter of the ablated region under laser irradiation was evaluated both theoretically and experimentally.

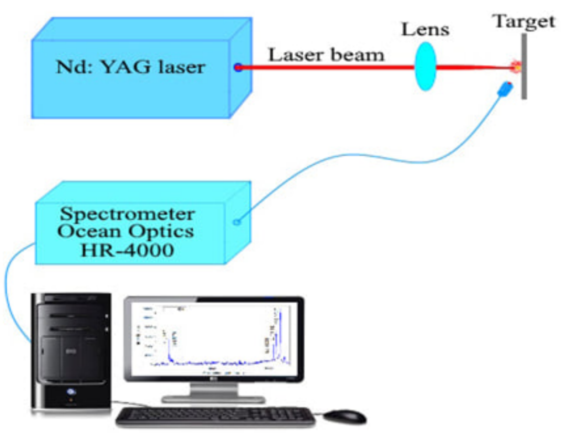

Figure 1. Schematic of the experimental setup

In future studies, expanding the experimental configuration with time-resolved diagnostics, such as gated ICCD or streak cameras, would allow detailed tracking of plasma evolution dynamics. This would provide a deeper understanding of how picosecond pulses drive fast ionization and relaxation mechanisms. Moreover, implementing environmental control (e.g., vacuum chambers or inert atmospheres) could isolate plasma effects from ambient air interactions, improving the repeatability and accuracy of results. Experiments on a broader range of materials, such as semiconductors and dielectrics, will further contextualize copper's behavior and support a comparative analysis of ablation thresholds and plasma generation efficiency under similar laser parameters.

3. RESULTS AND DISCUSSION

Neutral atomic transition lines of Cu I were identified in the plasma spectrum, and the free electron concentration was calculated using the Stark broadening method. This technique enables the determination of electron density and temperature by analyzing the broadening and shifting of spectral lines under the influence of electric fields within the plasma.The formed crater was also subjected to spectral analysis to evaluate the presence and influence of Rayleigh–Taylor instability and Marangoni convection.

3.1. Determination of electron density and temperature

In the plasma spectrum generated on the surface of the copper foil under laser irradiation, the characteristic atomic transitions of the neutral copper atoms (Cu I) were identified (FIG 2). The identification of atomic emission lines corresponding to the plasma spectrum was carried out using data from the NIST atomic spectra database [33].

Determining the electron density is of critical importance in the study of plasma formed under laser irradiation. This work employed the Stark broadening method to estimate the electron density. Stark broadening refers to the widening and shifting of spectral lines caused by electric fields within the plasma, and it serves as a key phenomenon that enables the quantitative evaluation of free electron density.

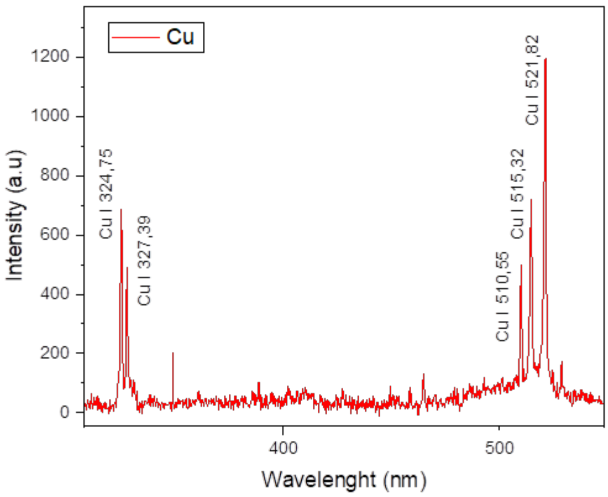

Figure 2. Plasma emission spectra of copper foil

The analysis of neutral copper atomic transition lines enabled precise characterization of plasma parameters, thereby providing a deeper understanding of laser ablation and its associated processes. For non-hydrogen-like atoms, the relationship between electron density and spectral lines' full width at half maximum (FWHM) is determined through Stark broadening [34].

$$\Delta\lambda_{\frac{1}{2}} = 2W\left(\frac{n_e}{10^{16}}\right)\mathring{A}\,, \tag{2}$$

Here, $\Delta\lambda_{1/2}$=FWHM denotes the full width at half maximum of the spectral line, n_e is the electron density, and W is the electron impact parameter. Electron densities were determined using the spectral wavelengths corresponding to Cu I atomic transitions via the Stark broadening method (Table 1). The FWHM values were obtained by fitting the spectral line profiles to a Voigt function (Fig. 3). Closely spaced atomic transitions were resolved and analyzed separately. Using the electron impact parameter W as reported in [35], the electron density n_e was calculated accordingly.

In the plasma field, the electron temperature is typically determined under the Local Thermodynamic Equilibrium (LTE) assumption. For a plasma in LTE, the population of particles' energy levels (excited states) follows the Boltzmann distribution law. According to the LTE condition, the Boltzmann plot method is expressed as follows [36, 37].

$$\ln\left(\frac{I_\lambda}{gA}\right) = -\frac{E_u}{k_B T_e} + \text{const}$$

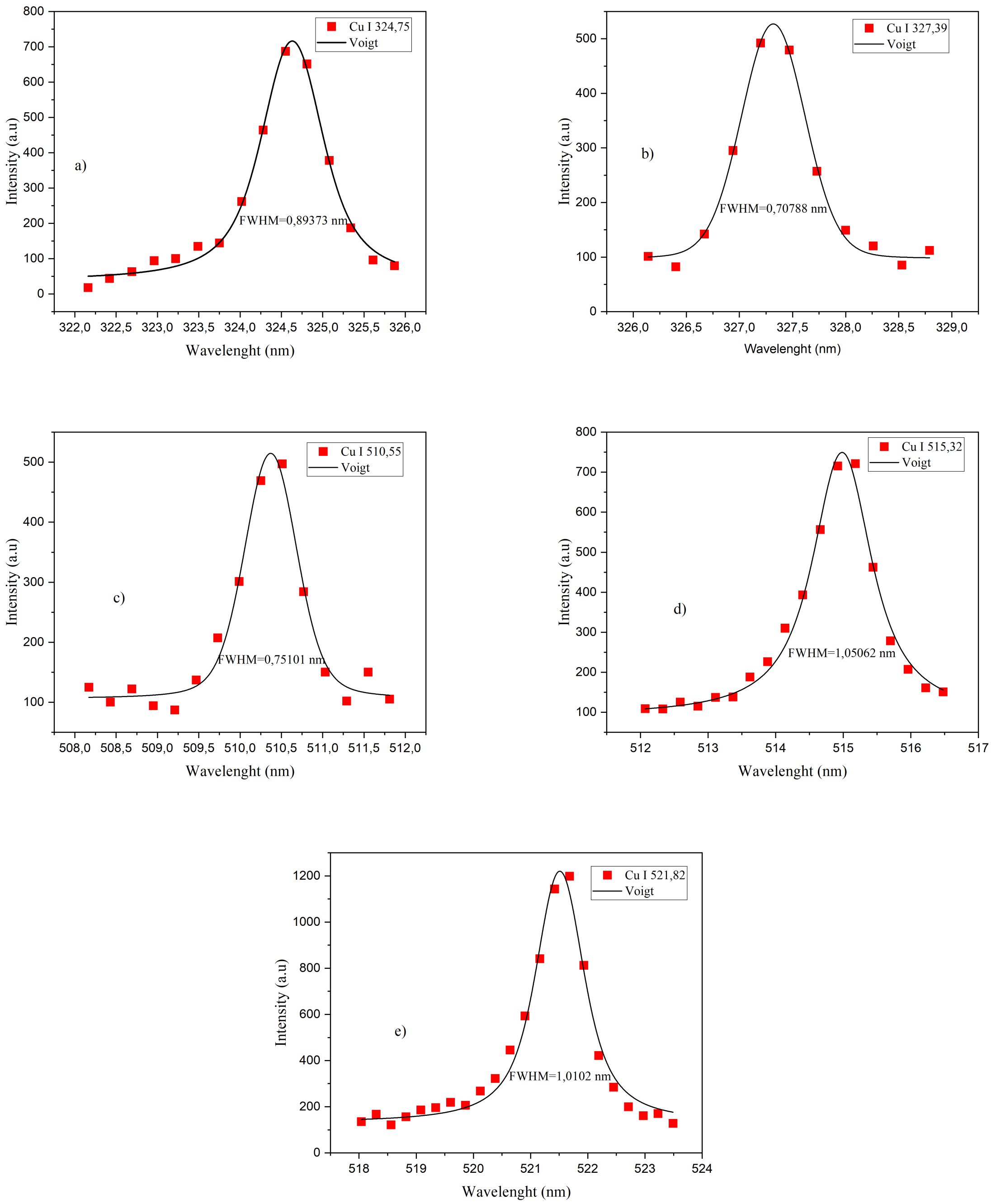

Figure 3. Voigt fitting of spectral lines in the plasma formed on the Cu surface: a) $\lambda = 324.75nm$, b) $\lambda = 327.39nm$, c) $\lambda = 510.55nm$, d) $\lambda = 515.32nm$, e) $\lambda = 521.82nm$.

Table 1. Experimental data table for Copper (Cu) element

Atom/ion	λ (nm)	FWHM (nm)	T (K)	w (Å)	n_e (10^{18} cm^{-3})
Cu I	324.75	0.89		0.003	14.84
Cu I	327.39	0.70		0.003	11.76
Cu I	510.55	0.75	8825	0.043	0.87
Cu I	515.32	1.05		0.19	0.27
Cu I	521.82	1.01		0.22	0.23

The intensity of the spectral line (I), wavelength (λ), statistical weight of the upper level (g), Einstein coefficient (A), energy of the upper level (E_u), Boltzmann constant (k_B), and electron temperature of the plasma (T_e) are the main parameters involved. The values of the parameters required to determine the electron temperature are taken from the

NIST [33] database, as presented in Table 2.

Atom	$\lambda_{ki,Z}$ (nm)	**Upper Level Energy** E_k (cm^{-1})	**Upper-state degeneracy** g_k	**Einstein coefficients** A_{ki} (s^{-1})
Cu I	324.75	30783.697	4	1.39×10^8
Cu I	327.39	30535.324	2	1.376×10^8
Cu I	510.55	30783.697	4	2×10^6
Cu I	515.32	49935.195	4	6×10^7
Cu I	521.82	49942.051	6	7.5×10^7

Table 2. Experimental Data Table for Copper (Cu) Element

The left-hand side of the linear equation based on the Boltzmann distribution is given by $\ln\left(\frac{I\lambda}{gA}\right)$. When several transitions to higher energy levels are considered for particles in the same ionization stage (Z), the left-hand side becomes proportional to the inverse of the electron temperature, $-1/(k_B T_e)$. This method, which relies on spectroscopic data, provides high accuracy in determining the plasma state, particularly the electron temperature. In plasma diagnostics, the electron temperature is not merely a numerical value; rather, it is a key parameter that characterizes the internal energy state of the plasma. Accurate temperature determination allows for precise conclusions regarding the plasma properties, such as the degree of ionization, charge carrier density, and other dynamic characteristics.

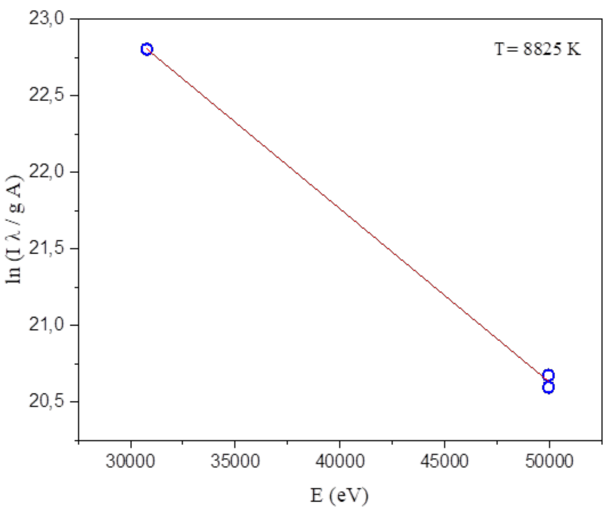

Figure 4. Emission spectral lines of neutral copper atom (Cu I) transitions plotted on a Boltzmann distribution graph

The plasma temperature was estimated using the Boltzmann plot method based on the intensities and energy levels of various Cu I spectral lines. The determined plasma temperature was approximately 8825 K. The electron density was observed to range from 0.23×10^{18} cm^{-3} to 14.84×10^{18} cm^{-3}, with the highest value corresponding to the spectral line at 324.75 nm (Fig. 4).

3.2. Crater morphology

The image of the crater formed as a result of laser ablation was obtained using a Scanning Electron Microscope (SEM). The laser radiation with a wavelength of 1064 nm (infrared) is significantly absorbed by the copper (Cu) foil. The pulse duration of 28 picoseconds (ps) is extremely short, meaning the metal heats rapidly under laser exposure, leading to vaporization. A laser fluence of 16 J/cm^2 is sufficient to initiate local melting and vaporization on the surface of the foil.

When the laser radiation interacts with the foil surface, the outer electrons of copper atoms transition to higher energy states, resulting in localized heating. Due to the laser energy being concentrated in a very small area, the material melts rapidly. The short pulse duration limits thermal diffusion into the bulk material, causing heat to accumulate primarily at the surface. This process is associated with hot electron diffusion, which confines thermal energy within the near-surface region.

If the laser energy is sufficiently high, the copper layer melts and part of it immediately vaporizes. At high vaporization rates, a plasma regime is established. The vaporized particles expand from the surface, interact with ambient air molecules, and cool and condense. As a result of these processes, a crater is formed on the Cu foil surface (Fig 5).

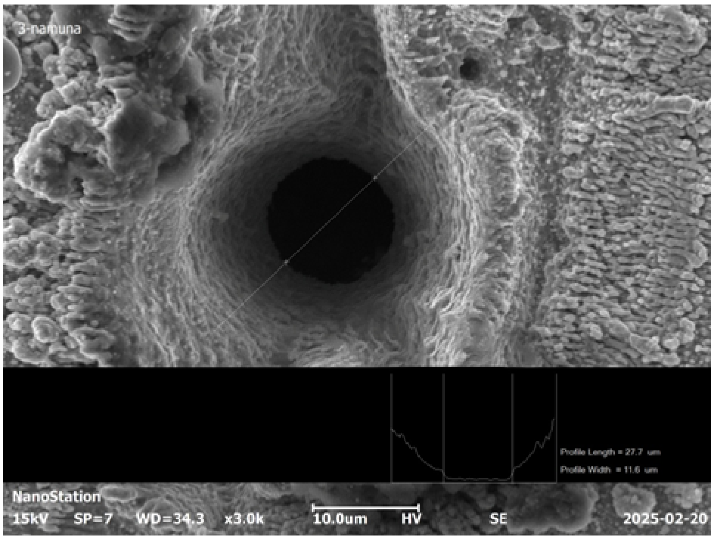

Figure 5. Scanning Electron Microscope (SEM) image of a crater formed on a copper foil surface (crater depth: 11.6 μm)

A model based on the Gaussian intensity profile of the laser beam is considered to estimate the crater diameter or the expansion of the ablated region during laser ablation. In this profile, the laser intensity is maximal at the center and decays exponentially with radial distance [38].

The spatial distribution of laser intensity follows a Gaussian profile:

$$I(r) = I_0 \cdot \exp\left(-\frac{2r^2}{\omega^2}\right), \tag{3}$$

where I_0 is the peak intensity at the center ($r = 0$), ω is the beam radius at $1/e^2$ intensity level, and r is the radial distance from the center.

Ablation occurs only when the local fluence exceeds a threshold value E_0. Solving for the radial position r where $E(r) = E_0$, the ablated diameter D can be expressed as:

$$D = a \cdot \omega \cdot \sqrt{2 \ln\left(\frac{E}{E_0}\right)}, \tag{4}$$

where a is an empirical correction factor close to 1, accounting for beam geometry and experimental conditions.

This model reveals that the relationship between laser fluence and crater diameter is not linear but logarithmic. Hence, doubling the laser energy fluence does not double the crater diameter; the growth is proportional to $\ln(E)$.

Two key effects are considered in understanding the morphology of the crater and its surrounding surface texture. Circular-shaped craters were observed to form, and the laser fluence and pulse duration directly influenced their dimensions and geometries. The ablation radius was calculated based on the logarithmic relationship between fluence and the ablation threshold, in agreement with previously published studies [39]. The crater rim exhibits signs of resolidification and material redistribution, driven by thermal gradients and recoil pressure.

3.3. Quantitative analysis of molten-layer dynamics and Rayleigh–Taylor instability

When intense picosecond laser radiation interacts with a metallic foil, rapid energy deposition leads to surface vaporization and plasma formation. In the central region of the laser spot, where the local fluence is maximal, material removal is dominated by explosive ablation. In contrast, in the peripheral region of the spot the fluence decreases below the ablation threshold, resulting primarily in transient surface melting accompanied by lateral molten flow. Under such conditions, the appearance of periodic ripple-like or finger-shaped structures at the crater edge is commonly attributed to hydrodynamic instabilities developing within the molten layer, most notably the Rayleigh–Taylor instability (RTI) [40,41].

The Rayleigh–Taylor instability arises at an interface between two media of different densities when the denser layer is accelerated toward the lighter one. In the case of laser ablation, this configuration naturally occurs at the molten metal–plasma (or vapor) interface, where the dense molten copper layer is subjected to a strong outward acceleration driven by the plasma pressure gradient. Small perturbations at this interface may therefore grow in time, leading to characteristic ripple or finger-like morphologies upon resolidification.

3.3.1. Experimental input parameters Plasma parameters were determined using optical emission spectroscopy. The electron temperature was found to be $T_e \approx 8825$ K, while the electron density varied in the range $n_e = (0.23–14.84) \times 10^{18}$ cm^{-3}, depending on the selected Cu I emission line. Assuming local thermodynamic equilibrium and using the ideal gas approximation, the plasma pressure corresponding to each spectral line was calculated as

$$P = n_e k_B T_e. \tag{5}$$

Among the analyzed transitions, the Cu I line at 324.75 nm yielded the highest pressure, $P = 1.88 \times 10^6$ Pa, which was adopted as a representative value characterizing the maximum plasma loading acting on the molten surface. High-resolution SEM observations of the crater periphery revealed a well-defined periodic surface modulation. Statistical analysis over a 10 μm field of view containing multiple periods yielded a dominant wavelength

$$\lambda = (0.91 \pm 0.10)\ \mu\text{m}, \tag{6}$$

corresponding to a perturbation wavenumber

$$k = \frac{2\pi}{\lambda} \approx 6.9 \times 10^6\ \text{m}^{-1}. \tag{7}$$

3.3.2. Molten-layer thickness and lifetime estimation In the picosecond laser irradiation regime, the extremely short pulse duration confines heat transport to a narrow near-surface region, thereby suppressing significant thermal diffusion into the bulk material. As a result, laser energy deposition leads to the formation of a transient molten layer characterized by an effective thickness L. The temporal evolution and persistence of this molten phase are primarily governed by thermal diffusion and can be estimated using a characteristic diffusion timescale,

$$t_{\text{eff}} \sim \frac{L^2}{\alpha}, \tag{8}$$

where α denotes the thermal diffusivity of copper, taken as $\alpha \approx 1.0 \times 10^{-4}$ m^2 s^{-1}.

Assuming a physically realistic molten-layer thickness in the range $L = 1–5$ μm, the corresponding molten-layer lifetime is estimated to fall within

$$t_{\text{eff}} \sim 10–250\ \text{ns}. \tag{9}$$

This nanosecond-scale lifetime significantly exceeds the laser pulse duration and establishes a well-defined temporal window during which the molten layer remains dynamically active. Such a timescale is sufficient to permit the initiation and growth of interfacial hydrodynamic instabilities at the molten metal–plasma interface, thereby providing favorable conditions for the emergence of instability-driven surface modulations and complex crater-edge morphologies (Fig 6).

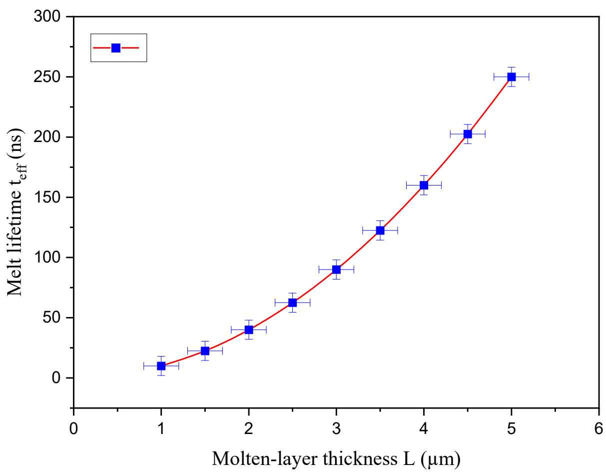

Figure 6. Dependence of the molten-layer lifetime t_{eff} on the molten-layer thickness L. The experimental data with error bars are well fitted by a quadratic function, indicating a diffusion-controlled thermal relaxation process governing the transient molten phase.)

3.3.3. Rayleigh–Taylor instability growth For a molten layer of finite thickness, the growth rate of the Rayleigh–Taylor instability can be expressed as [40, 41]

$$\gamma_{\mathrm{RTI}} = \sqrt{\frac{A g_{\mathrm{eff}} k}{1 + AkL}}, \tag{10}$$

where $A = (\rho_1 - \rho_2)/(\rho_1 + \rho_2)$ is the Atwood number, k is the perturbation wavenumber, and g_{eff} is the effective acceleration acting at the interface. Since the density of molten copper is several orders of magnitude larger than that of the plasma or vapor phase, the Atwood number can be reasonably approximated as $A \approx 1$.

The effective acceleration is governed by the plasma-induced pressure gradient acting on the molten layer and may be estimated as

$$g_{\mathrm{eff}} \simeq \frac{\Delta P}{\rho_h L}, \tag{11}$$

where $\rho_h \approx 8000\ \mathrm{kg\,m^{-3}}$ is the density of molten copper.

Using the experimentally determined plasma pressure and the measured perturbation wavelength, the characteristic RTI growth time, $\tau_{\mathrm{RTI}} = \gamma^{-1}$, is found to lie in the range

$$\tau_{\mathrm{RTI}} \sim 70\text{–}330\ \mathrm{ns}, \tag{12}$$

depending on the assumed molten-layer thickness.

3.3.4. Physical interpretation and role of thermal gradients The close correspondence between the characteristic growth time of the Rayleigh–Taylor instability, τ_{RTI}, and the effective lifetime of the molten layer, t_{eff}, provides compelling evidence that RTI can fully evolve within the transient molten phase generated by picosecond laser irradiation. This temporal compatibility is not merely qualitative but quantitatively confirms that the molten copper layer persists long enough for interfacial perturbations to amplify under the action of an effective acceleration field. Consequently, the experimentally observed sub-micrometer ripple patterns and finger-like protrusions formed at the crater periphery can be consistently attributed to RTI-driven deformation at the liquid–solid interface during the molten stage.

Beyond the pressure-induced instability mechanism, the laser–matter interaction inherently establishes an extreme thermal gradient between the hot laser-induced plasma and the comparatively cold bulk material beneath the surface. This gradient may be estimated using

$$\nabla T = \frac{T_{\mathrm{plasma}} - T_{\mathrm{ambient}}}{\Delta x}, \tag{13}$$

where the plasma temperature can be reasonably approximated by the electron temperature ($T_{\mathrm{plasma}} \approx T_e$), the ambient temperature is taken as $T_{\mathrm{ambient}} \approx 300$ K, and Δx denotes the characteristic depth over which the temperature drop occurs. In the picosecond regime, where thermal diffusion is strongly confined to the near-surface region, this depth can be safely approximated by the molten-layer thickness, such that $\Delta x \approx L$.

Under these conditions, the resulting temperature gradient reaches values on the order of 10^9–$10^{10}\ \mathrm{K\,m^{-1}}$, signifying the presence of extremely strong thermocapillary forces at the molten surface. Such gradients are sufficient to drive intense Marangoni convection, promoting lateral melt flow and additional redistribution of molten material. Although these thermally driven flows are not explicitly included in the analytical formulation of the RTI growth rate-where the dominant contribution arises from the pressure-induced effective acceleration-they are expected to play a complementary role. Specifically, Marangoni convection can act synergistically with RTI by modifying the local melt thickness and enhancing the nonlinear evolution of interfacial perturbations.

Taken together, these results suggest that the final surface morphology observed after resolidification is governed by the combined action of pressure-driven Rayleigh–Taylor instability and thermocapillary melt flow. While RTI provides the primary mechanism for pattern initiation and wavelength selection, the strong temperature-gradient-induced Marangoni convection contributes to the amplification and lateral modulation of surface features, leading to the complex crater-edge structures observed experimentally [42–44].

3.4. Marangoni convection

When a solid metal surface is exposed to high-power picosecond laser irradiation, the deposited energy is absorbed within an extremely shallow near-surface region, leading to an ultrafast and highly localized temperature rise. Under these conditions, the surface layer rapidly enters a molten state and may partially ionize, resulting in the formation of a laser-induced plasma above the target. Owing to the short pulse duration and the correspondingly limited thermal diffusion length, heat transport into the bulk material is strongly suppressed. As a consequence, the temperature field within the molten metal layer becomes highly nonuniform, exhibiting steep thermal gradients between the intensely heated central region and the cooler peripheral zones.

Such pronounced thermal inhomogeneity naturally gives rise to Marangoni convection, a thermocapillary-driven flow mechanism originating from spatial variations in surface tension along the molten surface [11, 13]. In metallic melts, surface tension generally decreases with increasing temperature, implying that temperature gradients are directly converted

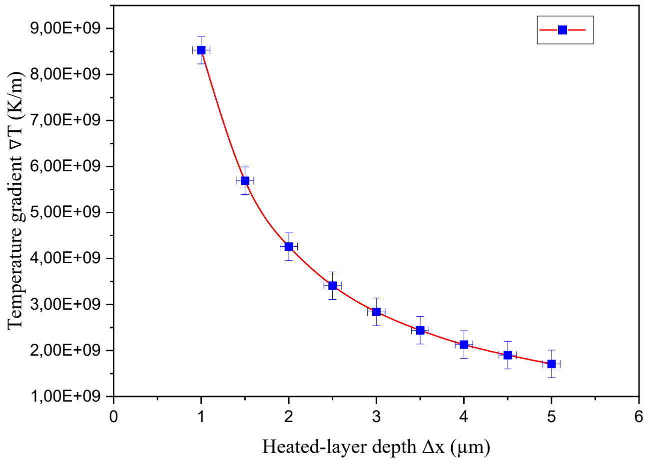

Figure 7. Dependence of the temperature gradient ∇T on the heated-layer depth Δx. The experimental data with error bars are well described by an inverse relationship, $\nabla T \propto 1/\Delta x$, indicating the presence of a steep thermal gradient within the laser-heated near-surface region.)

into surface-tension gradients. As a result, molten material is driven from regions of lower surface tension (hot zones) toward regions of higher surface tension (cooler zones), leading to an efficient lateral redistribution of the melt during the laser–matter interaction [45].

The thermocapillary driving force associated with Marangoni convection can be expressed as

$$\nabla\sigma = \frac{d\sigma}{dT}\nabla T, \tag{14}$$

where $\nabla\sigma$ denotes the surface-tension gradient, $\frac{d\sigma}{dT}$ is the temperature coefficient of surface tension, and ∇T represents the temperature gradient across the molten layer. For molten copper, the temperature coefficient of surface tension is negative, $\frac{d\sigma}{dT} \approx -0.3 \times 10^{-3}\ \mathrm{N\,m^{-1}\,K^{-1}}$, indicating that the thermocapillary flow is directed radially outward from the laser-heated center toward the cooler periphery.

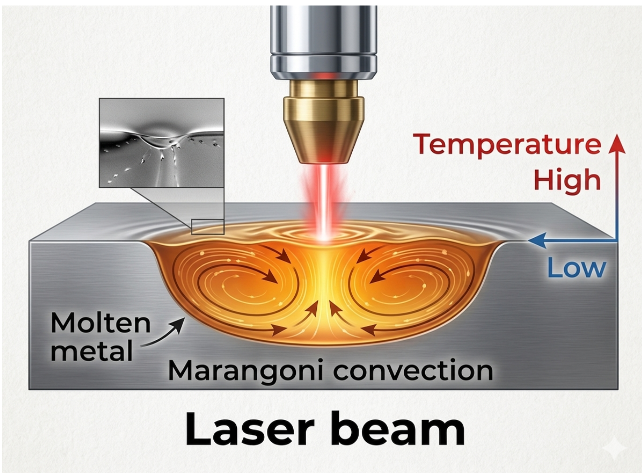

Figure 8. Schematic illustration of Marangoni convection induced by strong temperature gradients on the molten metal surface during picosecond laser irradiation.

Figure 8 schematically illustrates the development of Marangoni convection during laser irradiation. As the surface temperature gradient increases, the associated surface-tension gradient becomes stronger, giving rise to more intense thermocapillary flow. This flow substantially modifies the melt-pool geometry and plays an important role in determining the final crater morphology after resolidification, which may range from nearly axisymmetric to strongly distorted depending on the balance between convective transport and solidification dynamics.

The relative importance of Marangoni convection can be quantitatively assessed using the dimensionless Marangoni number (Ma), which characterizes the ratio of thermocapillary driving forces to viscous dissipation:

$$Ma = \frac{\left|\frac{d\sigma}{dT}\right| \Delta T\, L}{\mu\, \alpha}, \tag{15}$$

where ΔT is the characteristic temperature difference across the molten layer, L is the effective molten-layer thickness, μ is the dynamic viscosity of the molten metal, and α is the thermal diffusivity.

The importance of the surface-tension coefficient in determining crater morphology has also been confirmed under other pulsed irradiation techniques. Zhong et al. [15] demonstrated that differences in the surface-tension coefficient between molten inclusions and the surrounding molten matrix generate strong thermocapillary flow, ultimately controlling crater evolution during intense pulsed ion beam irradiation. Although the present study employed high-purity copper foil, where impurity effects are expected to be minimal, the reported mechanism emphasizes that even small compositional variations may alter Marangoni convection through local changes in the temperature coefficient of surface tension ($d\sigma/dT$). Therefore, the purity of the target material should be regarded as an important parameter affecting crater morphology.

Based on experimentally inferred plasma and surface temperatures, the peak temperature in the laser-irradiated region reaches approximately $T_{\text{plasma}} \approx 8.8 \times 10^3$ K, while the surrounding material remains close to ambient conditions, $T_{\text{ambient}} \approx 300$ K. This yields a temperature difference of $\Delta T \approx 8.5 \times 10^3$ K. Taking a molten-layer thickness consistent with the RTI analysis, $L = 1$–5 μm, together with a dynamic viscosity of molten copper $\mu \approx 4.3 \times 10^{-3}$ Pa·s and a thermal diffusivity $\alpha \approx 1.1 \times 10^{-5}$ m^{2}s^{-1}, the Marangoni number is estimated to lie in the range

$$Ma \sim (5 \times 10^4)\text{–}(3 \times 10^5). \tag{16}$$

This relatively large Marangoni number indicates that thermocapillary convection plays a dominant role compared to purely diffusive heat transport within the molten layer. Under such conditions, surface-driven flows are expected to redistribute molten material on nanosecond time scales, thereby significantly influencing melt-pool dynamics and the resulting surface morphology. Similar ranges of Marangoni numbers have been reported in previous experimental and numerical studies of laser-induced melt flows in metals, confirming that Marangoni convection constitutes a key mechanism governing crater-edge accumulation and material redistribution in pulsed laser ablation [46].

Furthermore, the interaction between Marangoni convection and other hydrodynamic instabilities, such as the Rayleigh–Taylor instability, further enhances the complexity of molten-layer dynamics. While RTI primarily governs the vertical deformation of the molten interface under plasma-induced effective acceleration, Marangoni convection introduces strong lateral transport. Together, these mechanisms act synergistically to shape the final resolidified surface features observed experimentally.

A comparison with previous investigations suggests that the physical mechanisms governing crater formation are largely independent of the irradiation source. Bryukhovetsky et al. [14] attributed crater formation under pulsed electron-beam irradiation to non-uniform crystallization of the remelted surface layer, whereas Zhong et al. [15] emphasized the role of impurity-induced surface-tension differences during pulsed ion beam irradiation. In contrast, the present work demonstrates that for high-purity copper irradiated by picosecond laser pulses, crater morphology is mainly controlled by the combined action of Rayleigh–Taylor instability and Marangoni convection. Thus, while the dominant driving force varies depending on the irradiation technique and material characteristics, hydrodynamic melt flow remains the key factor governing crater evolution.

4. CONCLUSIONS

Within the scope of this study, the physical phenomena induced by laser irradiation on metallic surfaces were systematically investigated. In particular, processes such as plasma formation under laser pulse exposure, surface flows within the molten layer, instabilities, and crater formation were analyzed theoretically and experimentally in depth. Key parameters such as laser power, pulse duration, spot radius, and material properties (e.g., viscosity and thermal diffusivity) were carefully considered.

Based on the analysis of plasma spectra using the Voigt profile, the temperature was estimated as $T \approx 8825$ K, and the electron densities derived from several spectral lines were found to be on the order of $n_e \sim 10^{18}$ cm^{-3}, indicating a dense and high-energy plasma state. This suggests a high intensity of energy exchange in the laser–material interaction.

The temperature gradients formed at the plasma–melt interface are strongly associated with the temperature dependence of surface tension, which leads to pronounced Marangoni convection. According to calculations, the Marangoni number was approximately $Ma \approx 5.4 \times 10^5$, implying that convective transport dominates surface diffusion. These flows play a crucial role in redistributing the molten metal from the center to the periphery, thereby shaping the crater geometry.

Furthermore, the density differences induced within the material by laser irradiation triggered Rayleigh–Taylor instability. This instability leads to the emergence of irregular internal structures, concentration gradients, and an unstable evolution of the surface morphology. As a result of the combination of such instabilities and convective flows, the crater shape, depth, and radius formed by laser irradiation exhibit complex variability.

Comparison with previous studies employing pulsed electron and ion beams further confirms that crater formation is a universal consequence of coupled thermal transport, melt hydrodynamics, and solidification processes. However, the dominant mechanism may vary depending on material purity, alloy composition, irradiation source, and energy deposition conditions.

In conclusion, the research confirms the intricate nature of the processes occurring on metal surfaces under laser irradiation and highlights the importance of accurate modeling. The findings demonstrate that energy absorption, plasma dynamics, temperature gradients, instabilities, and internal flows influence crater formation. These results are essential for enhancing precision and quality in forming surface structures and craters using laser technologies.

ORCID

M.M. Akhmedov, https://orcid.org/0000-0003-1208-1736; **J.O. Sadullayev**, https://orcid.org/0000-0002-5577-2644; **M.E. Vapayev**, https://orcid.org/0009-0007-5194-131X; **N.P. Babayazova**, https://orcid.org/0009-0006-7877-2459; **A.R. Matnazarov**, https://orcid.org/0009-0000-7420-8742; **I.Y. Davletov**, https://orcid.org/0009-0006-5971-7649; **M. Jumaniyazova**, https://orcid.org/0009-0001-9809-3086; **R.O. Ozodov**, https://orcid.org/0009-0002-4878-6519; **B. Ismatov**, https://orcid.org/0000-0003-1283-8970; **F.J. Matchanova**, https://orcid.org/0009-0005-5194-5439

REFERENCES

[1] Japakov A. I. *et al*. "The impact of laser radiation frequency on the formation of the main characteristics of ions in a mono-element laser plasma," EPJ Web of Conferences, EDP Sciences, **318**, 05002 (2025). https://doi.org/10.1051/epjconf/202531805002

[2] Japakov A. I. *et al*. "Spectra of multiply charged ions in laser plasma formed from gas-containing targets,"East European Journal of Physics, (3), 490-494 (2023). https://doi.org/10.26565/2312-4334-2023-3-55

[3] Ruziev Z. *et al*. "Surface ionization of diamond by femtosecond laser pulses: A comparative study of analytical models," Results in Optics, **23**, 100942 (2026). https://doi.org/10.1016/j.rio.2025.100942

[4] Lian B. *et al*. "Research and experimentation on acoustic monitoring technology for laser drilling penetration," Micromachines, **16**(4), 475 (2025). https://doi.org/10.3390/mi16040475

[5] Hayasaki Y., and Miura T. "Femtosecond laser drilling controlled with laser-generated ultrasound pressure," Applied Physics B, **130**(12), 220 (2024). https://doi.org/10.1007/s00340-024-08355-1

[6] Sheng L. et al. "Investigation on cutting of CFRP composite by nanosecond short-pulsed laser with rotary drilling method," Science and Engineering of Composite Materials, **32**(1), 20240047 (2025). https://doi.org/10.1515/secm-2024-0047

[7] Boltaev G. S. *et al*. "Impact of plasma conditions on the shape of femtosecond laser-induced surface structures of Ti and Ni," Applied Physics A, **128**(6), 488 (2022). https://doi.org/10.1007/s00339-022-05614-w

[8] Eshchanov B. X. *et al*. "Ultrafast laser nanostructured silicon coated with silver nanoparticles for efficient SERS detection of R6G," Applied Physics A, **132**(2), 111 (2026). https://doi.org/10.1007/s00339-025-09179-2

[9] Vapaev M. E. *et al*. "Laser fluence-dependent LIPSS formed on the surface of niobium alloys," EPJ Web of Conferences. – EDP Sciences, **318**, 05005 (2025). https://doi.org/10.1051/epjconf/202531805005

[10] S. Singh, B. Vidhani, S. Yogi, A. Tyagi, S. Kumar, and S.K. Meena, *Plasma waves and Rayleigh–Taylor instability: Theory and application, Plasma Science-Recent Advances, New Perspectives and Applications*, (IntechOpen, 2023). https://doi.org/10.5772/intechopen.109965

[11] Hu K. *et al*., "Thermal-fluid modeling and physics-informed machine learning for predicting molten pool depth in single-layer multi-track fiber laser cladding," The International Journal of Advanced Manufacturing Technology, **135**(7), 3591-3613 (2024). https://doi.org/10.1007/s00170-024-14706-1

[12] Zheng G. *et al*. "A linearized hydrodynamic code for laser ablation and its application to laser pulse shaping for direct-drive fusion," Physics of Plasmas, **31**(10), 102705 (2024). https://doi.org/10.1063/5.0225382

[13] Dai D. *et al*. "Role of angular velocity on Marangoni convection shifting, heat accumulation, and microstructure evolution using laser directed energy deposition," Journal of Applied Physics, **135**, 053105 (2024). https://doi.org/10.1063/5.0187045

[14] Bryukhovetsky V. V. *et al*. "Formation mechanism of craters on the surface of AA6111 aluminum alloy irradiated by quasi-relativistic high-current electron beam," Vacuum, **215**, 112263 (2023). https://doi.org/10.1016/j.vacuum.2023.112263

[15] Zhong H. *et al*. "Dynamic mechanism of crater formation induced by inclusion during intense pulsed ion beam irradiation," Vacuum, **179**, 109541 (2020). https://doi.org/10.1016/j.vacuum.2020.109541

[16] Tojinazarov F. *et al*. "Picosecond laser drilling grids in aluminium foil at 532 and 355 nm wavelengths," Engineering Research Express, **6**(1), 015050 (2024). https://doi.org/10.1088/2631-8695/ad1ea3

[17] Akhmedov M. *et al*. "Picosecond-pulsed laser ablation of aluminum foils: crater morphology and plasma parameters," Engineering Research Express, **7**(3), 035362 (2025). https://doi.org/10.1088/2631-8695/ae0092

[18] Akhmedov M. et al. "Effects of picosecond pulsed laser radiation on crater formation on copper foil surfaces," Engineering Research Express, **8**(3), 035401 (2026). https://doi.org/10.1088/2631-8695/ae3b9d

[19] Akhmedov M. *et al*. "Self-regulated crater formation governed by electron density in picosecond Nd: YAG laser-induced molybdenum plasma," Journal of Russian Laser Research, 1-15 (2026). https://doi.org/10.1007/s10946-026-10318-0

[20] Sadullayev J. O. *et al*. "Modeling of Thermal Effects in a Polyimide Target Under Pulsed Laser Irradiation," East European Journal of Physics, (1), 274-280 (2026). https://doi.org/10.26565/2312-4334-2026-1-31

[21] Sadullayev J. O. *et al*. "Finite Element Modeling of Scanning Speed Effects in Femtosecond Laser-Induced Graphene Fabrication," East European Journal of Physics, (2), 352-360 (2026). https://doi.org/10.26565/2312-4334-2026-2-37

[22] Ajith A. et al. "Comprehensive analysis of copper plasma: A laser-induced breakdown spectroscopic approach," Photonics, MDPI, 10(2), 199 (2023). https://doi.org/10.3390/photonics10020199

[23] Isaev M. S. *et al*. "The Surface Layer Morphology of Si¡ Cr¿ Samples," East European Journal of Physics, (4), 297-300 (2024). https://doi.org/10.26565/2312-4334-2024-4-32

[24] Isaev M. S. *et al*. "Study of the Inhomogeneities of Overcompensed Silicon Samples Doped with Manganese," East European Journal of Physics, (2), 341-344 (2024). https://doi.org/10.26565/2312-4334-2024-2-40

[25] Mamadalimov A. T. *et al*. "Study of Silicide Formation in Large Diameter Monocrystalline Silicon," East European Journal of Physics, (2), 366-371 (2024). https://doi.org/10.26565/2312-4334-2024-2-45

[26] Mustafoqulov A. *et al*. "Angular displacement measurement and control sensors of agricultural robot-manipulators," BIO Web of Conferences. – EDP Sciences, **105**, 03003 (2024). https://doi.org/10.1051/bioconf/202410503003

[27] Boboev A. Y. *et al*. "SRIM simulation of irradiation damage by protons in ZnO: S compound," Journal of Ovonic Research, **21**6, 781–788 (2025). https://doi.org/10.15251/JOR.2025.216.781

[28] Boboev, A. Y., Karimberdiev, U., Kadirov, S., Yunusaliyev, N. Y. "Growth of Solid Solutions $(Ge_2)(GaAs_{1-\delta}Bi_\delta)_x(ZnSe)_y$ on Silicon Substrates by Liquid Phase Epitaxy," Chalcogenide Letters, **22**(11), 951-957 (2025). https://doi.org/10.15251/CL.2025.2211.951

[29] Mamadalimov A. T. *et al*. "Comparative Analysis of the Properties of Manganese Silicide," Journal of Nano- and Electronic Physics, **17**(5), 05011 (2025). https://doi.org/10.21272/jnep.17(5).05011

[30] Qodirov S. R. U., and Davletov I. Y. "Improving thinking and imagining skills in school students by training the physics using simulations," AIP Conference Proceedings, **3268**(1), 060006 (2025). https://doi.org/10.1063/5.0257234

[31] Davletov I. *et al*. "Soft start of induction electric motors using rezistor and denistor devices," E3S Web of Conferences. – EDP Sciences, **461**, 01066 (2023). https://doi.org/10.1051/e3sconf/202346101066

[32] Davletov I. Y. *et al*. "Increasing the Efficiency of Asynchronous Motors by Improving the Quality of the Electric Current," in: *2023 IEEE XVI International Scientific and Technical Conference Actual Problems of Electronic Instrument Engineering (APEIE)*, (IEEE, 2023). pp. 1820-1824. https://doi.org/10.1109/APEIE59731.2023.10347842

[33] Kramida A., Ralchenko Y., and Reader J. "National Institute of Standards and Technology (NIST)," Atomic Spectra Database. 2022. https://physics.nist.gov/PhysRefData/ASD/lines_form.html

[34] Griem H. R. "Plasma spectroscopy in inertial confinement fusion and soft x-ray laser research," Physics of Fluids B: Plasma Physics, **4**(7), 2346-2361 (1992). https://doi.org/10.1063/1.860205

[35] Sahal-Bréchot S., Dimitrijević M. S., and Ben Nessib N. "Widths and shifts of isolated lines of neutral and ionized atoms perturbed by collisions with electrons and ions: An outline of the semiclassical perturbation (SCP) method and of the approximations used for the calculations," Atoms, **2**(2), 225-252 (2014). https://doi.org/10.3390/atoms2020225

[36] Harilal S. S. *et al*. "Optical diagnostics of laser-produced plasmas," Reviews of modern Physics, **94**(3), 035002 (2022). https://doi.org/10.1103/RevModPhys.94.035002

[37] Fikry M., Tawfik W., and Omar M. M. "Investigation on the effects of laser parameters on the plasma profile of copper using picosecond laser induced plasma spectroscopy," Optical and Quantum Electronics, **52**(5), 249 (2020). https://doi.org/10.1007/s11082-020-02381-x

[38] Zhang Z. *et al*. "Rule of the pulse energy from ground-based lasers for the laser ablation propulsion in space," Optics Express, **33**(6), 13439-13454 (2025). https://doi.org/10.1364/OE.554720

[39] Mohajan S., Beier N. F., and Hussein A. E. "Investigating crater formation in nanosecond laser ablation of aluminum foils," Journal of Applied Physics, **136**(2), 023102 (2024). https://doi.org/10.1063/5.0212660

[40] Suchandra P., and Ranjan D. "Dynamics of multilayer Rayleigh–Taylor instability at moderately high Atwood numbers," Journal of Fluid Mechanics, **974**, A35 (2023). https://doi.org/10.1017/jfm.2023.689

[41] Zhou Y. "Rayleigh–Taylor and Richtmyer–Meshkov instability induced flow, turbulence, and mixing. II," Physics Reports, **723**, 1-160 (2017). https://doi.org/10.1016/j.physrep.2017.07.008

[42] Xi C., and Xin T. "Heat transfer to a particle exposed to a rarefied plasma with a great temperature gradient," Journal of Thermal Science, **2**(2), 135-142 (1993). https://doi.org/10.1007/BF02718269

[43] Sun W. *et al*. "Numerical study of the effect of a magnetic field on Rayleigh-Taylor instability with different density disturbances," Frontiers in Physics, **11**, 1203081 (2023). https://doi.org/10.3389/fphy.2023.1203081

[44] Martins I. T., Gómez L. C., and Alvariño P. F. "Parametric investigation of Rayleigh–Taylor instability under experimental conditions with the lattice Boltzmann method," Physics of Fluids, **37**(2), 024131 (2025). https://doi.org/10.1063/5.0256018

[45] Onoda K., and Nanzai B. "Marangoni Convection Velocity in Nonlinear Hanging-Droplet Vibration Phenomena," Processes, **12**(3), 609 (2024). https://doi.org/10.3390/pr12030609

[46] Lin F. *et al*. "Marangoni convection-driven laser fountains on free surfaces of liquids," Materials Today Physics, **21**, 100558 (2021). https://doi.org/10.1016/j.mtphys.2021.100558

ТЕОРЕТИЧНИЙ ТА ЕКСПЕРИМЕНТАЛЬНИЙ АНАЛІЗ НЕСТАБІЛЬНОСТІ РЕЛЕЯ — ТЕЙЛОРА ТА КОНВЕКЦІЇ МАРАНГОНІ В МІДНІЙ ФОЛЬЗІ ПІД ДІЄЮ ЛАЗЕРНОГО ВИПРОМІНЮВАННЯ

М.М. Ахмедов[1], Дж.О. Садуллаєв[1], М.Є. Вапаєв[1], Н.П. Бабаязова[1], А.Р. Матназаров[2], І.Й. Давлетов[1], М. Джуманіязова[3], Р.О. Озодов[4], Б. Ісматов[5], Ф.Дж. Матчанова[6]

[1]*Кафедра техніки, Ургенчський державний університет імені Абу Райхана Беруні, Ургенч, 220100, Узбекистан*

[2]*Ургенчський інноваційний університет, вул. Міської Незалежності, 2-й будинок, Ургенч, 220100, Узбекистан*

[3]*Кафедра фізики та астрономії, Ургенчський державний педагогічний інститут, вул. Гурлан, 1-А, Ургенч, 220100, Узбекистан*

[4]*Кафедра біофізики, фізичної культури та спорту, Ургенчський державний медичний інститут. вул. Аль-Хорезмі, 2, Ургенч, 220100, Узбекистан*

[5]*Національний дослідницький університет "Ташкентський інститут інженерів іригації та механізації сільського господарства". Kori Niyoziy 39, Ташкент, 100000, Uzbekistan*

[6]*Хівська районна загальноосвітня середня школа № 10, вул. Саховат, 98, Хівський район, 220900, Узбекистан*

У цьому дослідженні вивчаються фізичні явища, що виникають на поверхні мідної фольги під дією високоінтенсивного імпульсного випромінювання Nd:YAG-лазера (λ = 1064 нм, τ = 28 пс), з особливим акцентом на утворенні плазми, нестабільності Релея — Тейлора (РТ) та впливі конвекції Марангоні на морфологію кратера. Температура плазми та електронна концентрація визначаються експериментальними методами за спектральними лініями випромінювання. Ці параметри дозволяють оцінити градієнт тиску в плазмі, температурні варіації та зміни поверхневого натягу. Нестабільність РТ моделюється на основі контрастів густини, що виникають за сильних перепадів тиску, тоді як конвекція Марангоні описується як механізм формування поверхневих потоків, зумовлених градієнтами температури. У роботі аналізується взаємодія між цими двома видами нестабільностей, їхня роль у перерозподілі матеріалу та вплив на кінцеву геометричну форму кратера, утвореного лазером, що підкріплюється теоретичними розрахунками та спектроскопічними вимірюваннями. Результати сприяють глибшому розумінню складних термогідродинамічних процесів, що супроводжують лазерну абляцію.

Ключові слова: *нестабільність Релея — Тейлора; конвекція Марангоні; лазерна абляція; мідна плазма; морфологія поверхні; електронна концентрація; спектроскопічна діагностика*